Changes in the crystallographic structures of cardiac myosin filaments detected by polarization-dependent second harmonic generation microscopy

Cai Yuan,[1] Zhonghai Wang,[1] Thomas K. Borg,[2] Tong Ye,[1] Catalin Baicu,[3] Amy Bradshaw,[3] Michael Zile,[3] Raymond B. Runyan,[4] Yonghong Shao,[5,6] and Bruce Z. Gao[1,*]

[1]*Department of Bioengineering, Clemson University, Clemson, South Carolina, 29634, USA*
[2]*Department of Regenerative Medicine and Cell Biology, Medical University of South Carolina Charleston, South Carolina, 29425, USA*
[3]*Department of Medicine, Medical University of South Carolina, Charleston, South Carolina, 29425, USA*
[4]*Department of Cell Biology and Anatomy, University of Arizona, Tucson, Arizona, 85724, USA*
[5]*College of Optoelectronics Engineering, Shenzhen University, Shenzhen, 518061, China*
[6]*shaoyh@szu.edu.cn*
**zgao@clemson.edu*

Abstract: Detecting the structural changes caused by volume and pressure overload is critical to comprehending the mechanisms of physiologic and pathologic hypertrophy. This study explores the structural changes at the crystallographic level in myosin filaments in volume- and pressure-overloaded myocardia through polarization-dependent second harmonic generation microscopy. Here, for the first time, we report that the ratio of nonlinear susceptibility tensor components d_{33}/d_{15} increased significantly in volume- and pressure-overloaded myocardial tissues compared with the ratio in normal mouse myocardial tissues. Through cell stretch experiments, we demonstrated that mechanical tension plays an important role in the increase of d_{33}/d_{15} in volume- and pressure-overloaded myocardial tissues.

1. Introduction

The crystallographic structure of cardiac myosin filaments is a major determinant of the strong binding of myosin heads to actin filaments and the accurate conformational changes in myosin heads mediating cardiac muscle-cell contraction. For example, the structural changes in myosin filaments under pathological hypertrophy have been thought to contribute to a binding mismatch between myosin and actin filaments. Second harmonic generation (SHG) microscopy is used to visualize myosin filaments without labeling [1,2]. The basic principle of this visualization is that the SHG signal is directly determined by the nonlinear susceptibility tensor, which is an optical property of the biomolecule (noncentrosymmetric biomolecules including, for example, myosin, collagen type I, and microtubule) associated with its crystal structure [3–5]. Polarization-dependent SHG microscopy is unique: It can retrieve the values of nonlinear susceptibility tensor components of a biomolecule and thus can be used to explore its crystallographic structure [3,6]. The relationship between the nonlinear susceptibility of myosin filaments and their crystallographic structures has been extensively studied. The values of nonlinear susceptibility tensor components of myosin filaments in different species are reportedly different [7], as are those values for the same myosin filaments in different physiological states (relaxed or contracted) [8,9].

Here, we report results of our study of the response of cardiac myosin filaments to pregnancy-induced volume overload and transverse-aortic constriction-induced pressure overload using polarization-dependent SHG microscopy. Compared with the values obtained in normal myocardia, the values of nonlinear susceptibility tensor components of myosin filaments in both volume- and pressure-overloaded myocardia increased significantly, suggesting changes in their crystallographic structure.

Because stretch reportedly can lead to structural changes in myosin filaments [10], we hypothesized that the value changes in the nonlinear susceptibility tensor components of myosin filaments in the two overload models would be triggered by mechanical tension. Mechanical tension in vivo can be decomposed into a longitudinal component (parallel with the long axis of the cells) and a lateral component (perpendicular to the long axis of the cells). Thus, we tested the above hypothesis using a cell stretch model. Our data demonstrated that the changes in the nonlinear susceptibility tensor values in myosin filaments observed in our cell-stretch models are compatible with those we detect in the volume- and pressure-overloaded myocardia.

2. Methods and materials

2.1 SHG and extraction of the components of the nonlinear susceptibility tensor

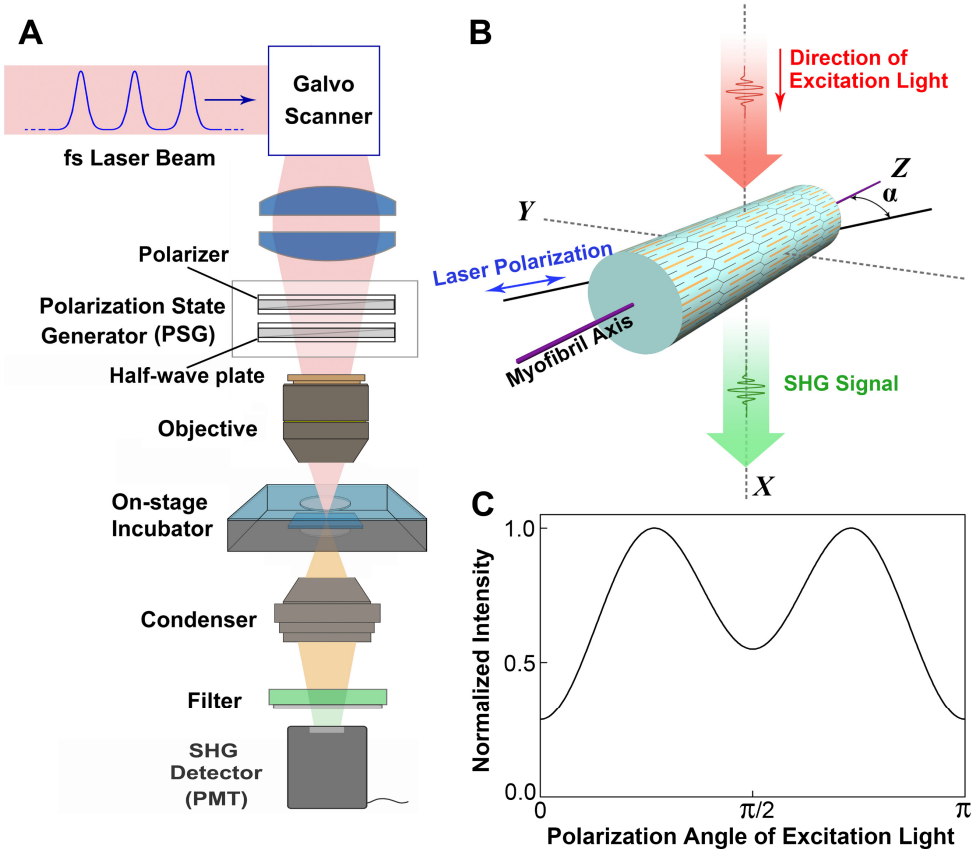

Fig. 1. (A) Experimental setup of the polarization-dependent SHG microscope. (B) Illustration of geometric arrangement of a single myofibril relative to the polarization of the applied excitation light field. α: the angle between the incident polarization of the excitation light and the z-axis (orientation of the myofibril). (C) The SHG signal intensity versus the polarization angle of the excitation light.

Conventionally, myosin is known to possess cylindrical symmetry (class C6) [4,7,11], which reduces the number of independent nonzero tensorial components of χ^2_{ijk}; d_{15}, d_{31}, and d_{33} are the only nonzero elements. If the Kleinman condition (the nonresonant character of the SHG scattering process) applies, only two tensor components among d_{15}, d_{31}, and d_{33} are independent: $d_{15} = d_{31}$ and d_{33} [12]. Figure 1(B) depicts the geometry that we consider for a single myosin myofibril relative to an applied excitation optical field. The SHG intensity ($I^{2\omega}$) and the polarization angle of the excitation light (α in Fig. 1(B)) satisfy the following C6-symmetry model [7,8]:

$$I^{2\omega} \sim \left[(\sin 2\alpha)^2 + \left(\frac{d_{31}}{d_{15}} \sin^2 \alpha + \frac{d_{33}}{d_{15}} \cos^2 \alpha \right)^2 \right] \quad (1)$$

Figure 1(C) is the polarization profile: The SHG signal intensity versus the polarization angle of the excitation light, which was plotted according to Eq. (1) (the specific tensor component settings are $d_{31} / d_{15} = 0.97$, $d_{33} / d_{15} = 0.69$ (Ref [7].)).

2.2 Polarization-dependent SHG imaging system

The construction of polarization-dependent SHG microscopy with an on-stage incubator is described in Fig. 1(A). The excitation laser beam was generated from a Ti:Sapphire laser (100 fs and 80 MHz, Tsunami 3960-X1BB pumped by a 9.5 W Millennia, Spectra-Physics) and was tuned to 830 nm. The beam was then steered onto the XY scanner (6210H, Cambridge Tech.). Before the beam was focused onto the sample using a 1.0 NA water immersion objective (60X LUMPlanFLN, Olympus), it passed a polarization state generator for rotating the polarization angle of the excitation light. The polarization state generator was composed of a polarizer (LPNIRE100-B, ThorLabs) that was mounted with an arbitrarily fixed polarization axis and a half-wave plate (WPH05M-830, ThorLabs) that was mounted on a motorized rotator (PRM1Z8, ThorLabs). By rotating the half-wave plate an angle of ψ relative to the fixed axis of the polarizer, the polarization of the excitation light would be rotated an angle of 2ψ without change in the intensity of the excitation light. During our experiments, at each imaging point, the half-wave plate was rotated to an orientation at which the SHG signal reached its minimum value. This orientation was selected as 0 degrees. The half-wave plate would be rotated to 85 degrees at every 5 degree interval so that the polarization of the excitation light would be rotated from 0 degrees to 170 degrees at every 10 degree interval. After the objective, the polarization ellipticity of the excitation light is >50:1, and the power of the excitation laser beam was set at 21 mw. This power is a little high for live cell culture; it was selected to ensure a high signal to noise ratio at the polarization corresponding to the spectral valley where in certain cases, the SHG is weak. The SHG signals were collected from the forward scattering direction through an Olympus 1.4 NA oil immersion condenser and recorded by a photomultiplier tube (H7422p-40, Hamamatsu). An IR filter was place in line before the photomultiplier tube and was used in addition to a 415 ± 15 nm bandpass filter (FF01-415/10-25, Semrock). The microscope stage and the objective mount were facilitated with motorized control mechanisms (MP-285, Sutter). In this study, the scan rate and the pixel dwell time were set to 500 lines/s and 3.2 μs, respectively, to achieve a 2D imaging rate of approximately one frame per second, where each frame contained 512 × 512 pixels with a pixel size of 0.16 μm. The lateral and axial resolution were experimentally estimated to be 0.47 and 1.26 μm, respectively [13].

All live cell imaging was performed in an on-stage incubator, which was composed of an electronically heated aluminum frame with feedback control and two covers (H301-TC1-HMTC, 2GF-MIXER, Okolab SRL, Ottaviano). A mixture of 95% air and 5% CO_2 was pumped through the heater unit, which contained deionized water, and the humidified air mixture (~37°C, 95% humidity) was supplied to the chamber of the on-stage incubator. By

design, the 5% CO_2 and 95% humidity mixture were maintained by adjusting the balance between the leakage and the supply through a feedback system. The 37°C temperature inside the culture dish was maintained by adjusting the balance between heat loss and gain through a feedback system including a temperature sensor placed inside the culture dish.

2.3 Sample preparation

In the research reported here, all myocardial samples were from three-month-old CD-1 mice. For the volume overload study, three-month-old pregnant mice was used, which were euthanized by the third day after delivery. For the pressure overload study, three two-month-old female mice first underwent the transverse-aortic contraction surgery previously described by Rockman and associates [14]. The mice were then fed normally for one-month, euthanized, and the hearts were harvested. The normal myocardial samples were from three-month-old normal female mice. Fifteen minutes prior to euthanasia, animals were given a 0.5 ml subcutaneous injection of 1:1000 heparin. Inhalation of 5% isoflurane was used to the animals to induce general anesthesia and 2.5% isoflurane was maintained during euthanasia. All uses of animals were approved by the Clemson University Institutional Animal Care and Use Committee.

The harvested hearts were immediately perfused with cardioplegia high k^+ solution to ensure all cardiomyocytes in the muscles were in a relaxed state and then fixed by 4% paraformaldehyde perfusion at zero transmural pressure and embedded in optimal cutting temperature (OCT) compound at –20 °C. To avoid variations due to possible regional heterogeneity, all slices were taken from the left ventricle free wall, and sections (10-μm thick) were cut using a cryostat (HM550, Thermo Scientific). The sliced samples were transferred to histology slides. Then, the OCT compound was washed away with PBS, and the samples were secured between two glass coverslips. Next, these samples were imaged under the polarization-dependent SHG microscope.

2.4 Cell culture and stretch

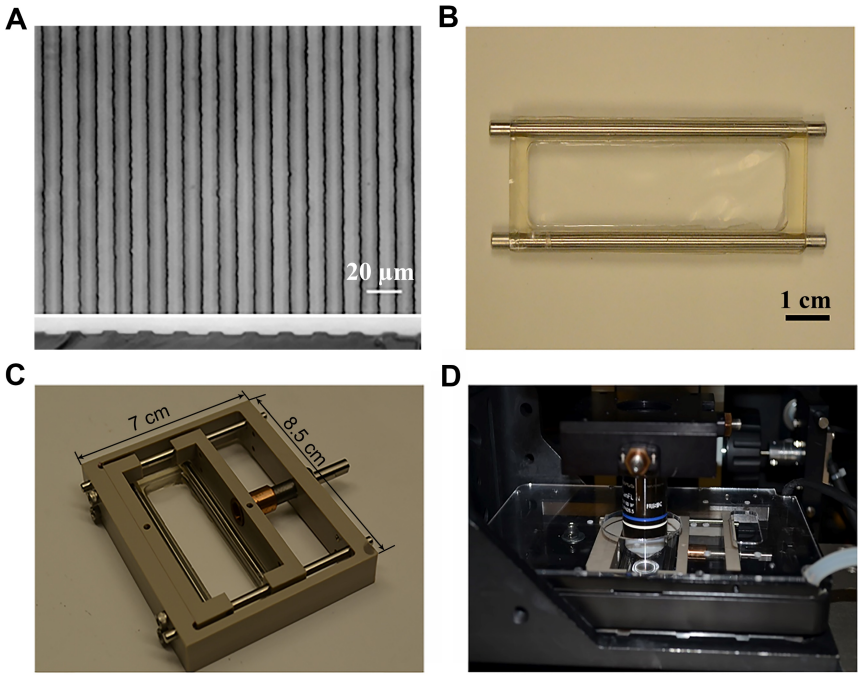

Fig. 2. (A) Grooved PDMS substrate for cardiomyocyte alignment and stretch delivery. (B) PDMS culture chamber, in which the grooved PDMS served as the bottom part. (C) Frame of

cell stretching device with culture chamber mounted. (D) Cell stretching device housed in the on-stage incubator.

Three-day-old Sprague-Dawley neonatal rats were euthanized according to a procedure approved by the Clemson University Institutional Animal Care and Use Committee. The cardiomyocytes were isolated and collected as previously described [15]. Briefly, the hearts were minced into 1 mm^3 pieces and first digested with trypsin solution (0.14 mg/mL without EDTA) overnight, then shaken at 75 rpm in a collagenase solution (1 mg/mL collagenase II, GIBCO; 0.24 U/mL neutral protease, Worthington) for 1.5 h. The fibroblasts were removed by pre-incubating the cells in a 150-cm^2 flask with the culture medium [DMEM solution containing 10% fetal bovine serum] for 2 h. The purified cardiomyocyte (~90%) suspension was diluted to 1 million cells/mL and then seeded into grooved PDMS substrate culture dishes coated with fibronectin (20 mg/mL) (Fig. 2(A)). Plating 2 mL of cells was sufficient to ensure a confluent monolayer of spontaneously contracting cells.

The stretcher design and the fabrication of the PDMS substrate in the research reported here are the same as those we used previously (Fig. 2(C)) [16]. The amount and duration of the stretch are based on papers studying mechanical stretch-induced cardiac hypertrophy [17,18].

In the study described here, grooved PDMS substrate was used to realize end-to-end cell alignment to mimic in vivo-like cell morphology, which was demonstrated to cause in vivo-like hypertrophy under stretch [16]. Two types of grooved PDMS substrate were designed: In one, the grooves were aligned with the stretching direction; in the other type, the grooves were perpendicular to the stretching direction. Multiple plates (e.g., PDMS chambers shown in Fig. 2(C)) of cells were prepared for the longitudinal and lateral stretch groups. After 48 hours of incubation, the plates of each group were instantly stretched 0%, 5%, 10%, 15% and 20%, respectively, and the stretches were sustained for 48 hours before SHG imaging to measure the values of the nonlinear susceptibility tensor components. For each stretch trial (e.g., 10% longitudinal stretch), five identical plates were studied with four arbitrarily selected points being polarization scanned to create 20 measurement points for each trial. In addition, to study the temporal response of the nonlinear susceptibility tensor components of myosin filaments, ten extra plates of cardiomyocytes were prepared, five for instant 15% longitudinal stretch and five for instant 15% lateral stretch after three days of incubation, and data were collected hourly after the stretch.

2.5 Image collection and analysis

In this study, before the SHG image scan, 16 mmol/L of potassium ions and 1.2 mmol/L of calcium ions were added to the culture medium to allow cardiomyocytes to be in a relaxed state. Images were collected at every 10 degree interval of the polarization angle of the excitation light, which started at 0 degrees and continued until the polarization angle reached 170 degrees. Then, we reversely collected another 18 images at every 10 degree interval starting at 170 degrees and continuing to the 0 degree polarization state. A stack formed by the collected images and the region of interest, 3 to 4 sarcomeres around a straight myofibril, was selected to calculate the average gray value in each image. The obtained data were fit to the model given by Eq. (1). To retrieve the ratios of the tensor components, we used a nonlinear least-squares method implemented in MATLAB with three parameters as specified d_{31}/d_{15} and $d_{33}/d_{15}$and a scale-factor. We developed a curve-fitting program based on the work published by Boulesteix and associates to estimate the length of myosin filaments [19], which is typically 1.6 μm. We used the full width at $1/e^2$ of the fitted SHG signal in a sarcomere as an estimation of the length of the myosin filaments. Although this estimation may not have been accurate, we used it consistently to compare the length of myosin filaments in various conditions.

2.6 Statistical analysis

In this paper, data are presented as mean ± standard deviation (SD). Statistical analysis was performed with SAS 9.4 software. One-way analysis of variance (ANOVA) tests were used to determine mean separation. Two-sample Student's t-tests were then performed on the average values. P values of <0.05 were considered to be significant.

3. Results

3.1 Cell and sarcomere morphology

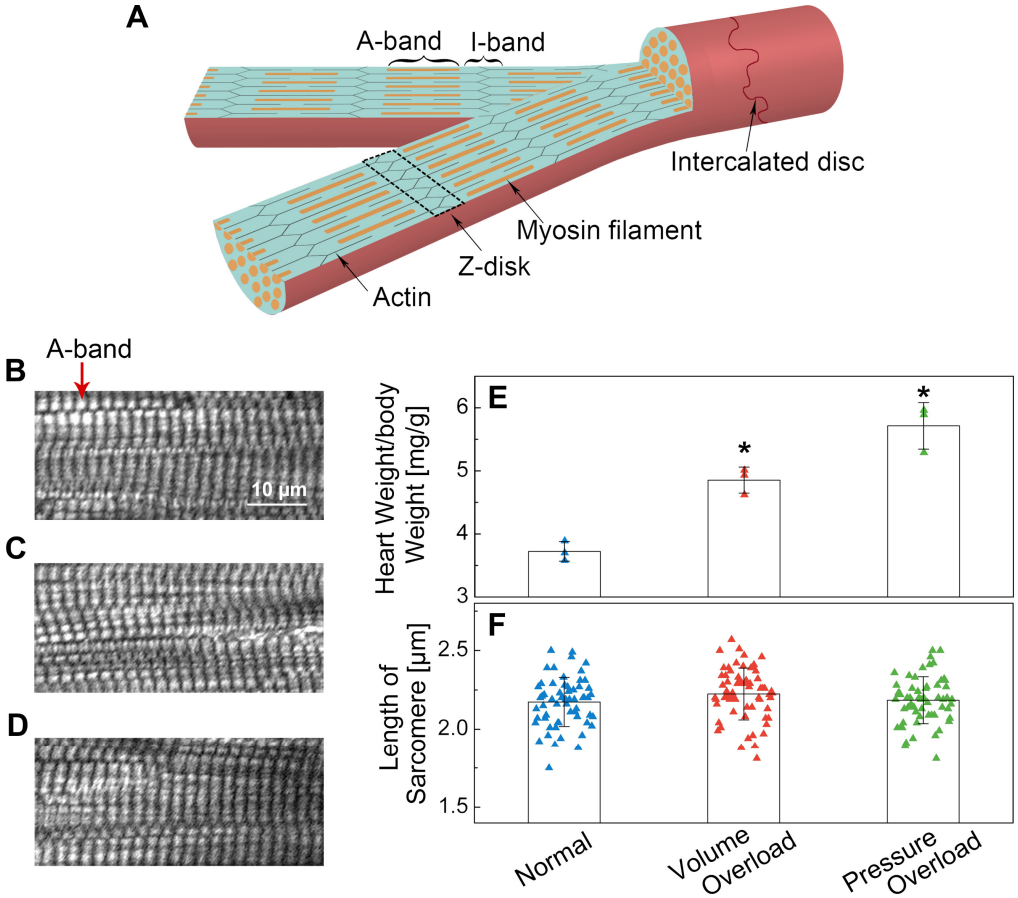

Fig. 3. (A) The arrangement of myosin filaments in a straight myofibril. The anisotropic band (A-band) is the region where myosin filaments and part of an actin filament are located; the isotropic region (I-band) is occupied partially by actin. Actin runs from the Z-disk to the center of the sarcomere. The Z-line is located in the ends of the sarcomere and defines the lateral boundaries of the sarcomere and anchors actin. (B)-(D) The linearly polarized SHG images of cardiomyocytes under (B) normal, (C) volume overload and (D) pressure overload conditions. (E) Bar plots of the heart weight to body weight ratios for normal, volume overload and pressure overload models were 3.73 ± 0.16 mg/g, 4.86 ± 0.21 mg/g and 5.72 ± 0.37 mg/g, respectively (sample size n = 3 mice/model. Bars represent mean ± SD. One-way ANOVA followed by Student's t-tests were used to compare different groups, *P < 0.05 vs. Normal). (F) Bar plots of sarcomeric length obtained from normal and volume- and pressure-overloaded myocardial samples: 2.17 ± 0.17 μm, 2.22 ± 0.20 μm and 2.19 ± 0.14 μm, respectively. (sample size n = 60 measurements/model: 10 tissue slides were arbitrarily selected from each mouse heart; 2 measurements were made for each slide. There was no statistical difference between the three mice in each group. Bars represent mean ± SD. There was no significant difference between groups (one-way ANOVA)).

Panels (B)-(D) in Fig. 3 are linear polarized SHG images that show uniformly distributed SHG intensities at each sarcomere in myocardial tissues from the normal and the volume- and pressure-overloaded models. A-bands are parallel to each other and evenly separated by I-bands. There is no significant morphological difference among the linear polarized SHG images obtained from normal cardiomyocytes and overloaded cardiomyocytes. Figure 3(E) presents the sample weights obtained immediately before and after heart harvest; the weights demonstrated significant increase in heart weight to body weight ratio under volume and pressure overload. Figure 3(D) shows the statistical result of the sarcomeric length measurements, which, based on Student's t-tests, demonstrates no significant difference ($p = 0.05$) although the average sarcomeric lengths in volume- and pressure-overloaded myocardial tissues showed slight increases.

3.2 Ratios of the 2nd-order nonlinear susceptibility tensor components

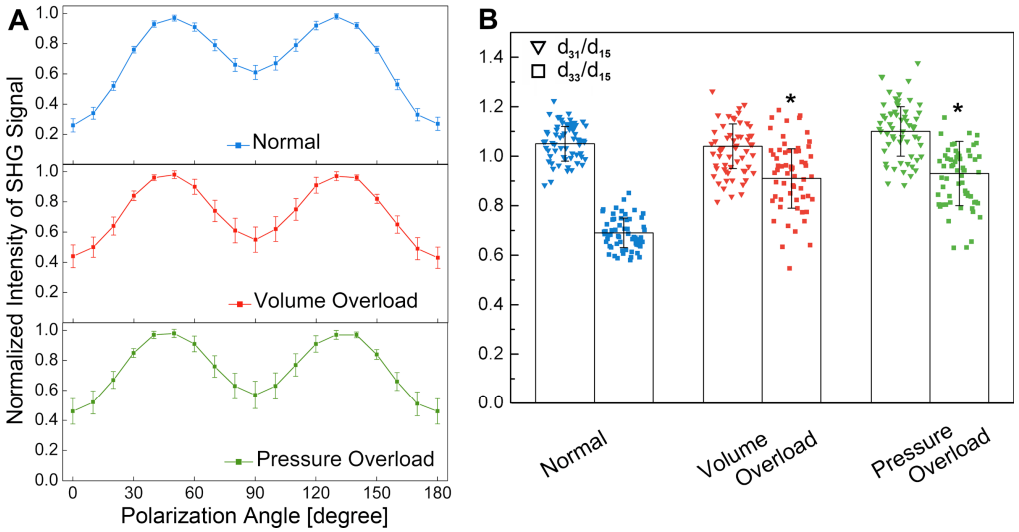

Fig. 4. (A) The polarization profiles of normal, volume- and pressure-overloaded myocardial tissues. (sample size n = 60 measurements/model: 10 tissue slides were arbitrarily selected from each mouse heart, and 2 measurements were made for each slide.) (B) Bar plots of the nonlinear susceptibility tensor components (d_{31}/d_{15}, and d_{33}/d_{15}) extracted from the measurement shown in (A): For myosin filaments from normal tissue, d_{31}/d_{15} value lies in the range of 1.05 ± 0.07 and d_{33}/d_{15}, 0.69 ± 0.06; for volume-overloaded myocardial tissues, d_{31}/d_{15} and d_{33}/d_{15} are 1.04 ± 0.09 and 0.91 ± 0.12, respectively; for pressure-overloaded myocardial tissues, the corresponding values are 1.10 ± 0.10 and 0.93 ± 0.13. (There was no statistical difference between the three mice in each group. Bars represent mean ± SD. One-way ANOVA followed by Student's t-test were used to compare different groups, *P < 0.05 vs. Normal.)

Figure 4(A) shows the polarization spectra from normal, volume- and pressure-overloaded myocardial tissues. The polarization spectra appear as a C6 symmetrical profile in all three cases. However, comparing the polarization spectrum from normal myocardial tissues with the spectra from volume- and pressure-overloaded myocardial tissues, we found that when the polarization angle is equal to 0 and 90 degrees, the corresponding intensities are different. These differences are reflected in the extracted ratio of the nonlinear susceptibility tensor components (Fig. 4(B)). The values of d_{31}/d_{15} in three cases were all around 1.00, showing no statistical difference under 0.05 confidence level. The values of d_{33}/d_{15} were significantly different ($p = 0.05$) between the normal and overloaded myocardial tissues although the values of d_{33}/d_{15} were not statistically different between the two overloaded myocardial tissues. Among all fits in this study, on average, the matching agreement between the data points and the fitting curve is $R^2 > 0.90$.

To explore the role of mechanical stretches that occur during volume overload and pressure overload in the changes in the ratio of the nonlinear susceptibility tensor components d_{33}/d_{15}, we studied the effect of simulated mechanical tension on the ratio of d_{33}/d_{15}. Figure 5 shows the data acquired from our cell culture model. In the absence of stretch, the value of d_{31}/d_{15} (0.99 ± 0.09) obtained from the cell culture was statistically the same as that obtained from normal myocardial tissues (Fig. 4(B)), while the value of d_{33}/d_{15} was 0.49 ± 0.05, which was significantly smaller than the value retrieved from normal myocardial tissues. With an increase in the stretch extent, the values of d_{31}/d_{15} in both longitudinal and lateral stretch models remained unchanged statistically, while the values of d_{33}/d_{15} increased significantly. When the stretches were increased to 20%, the values of d_{33}/d_{15} eventually reached 0.63 ± 0.05 for longitudinal stretch and 0.65 ± 0.06 for lateral stretch. Notably, as the stretch increased, especially when the stretch reached 20%, cell mortality increased significantly.

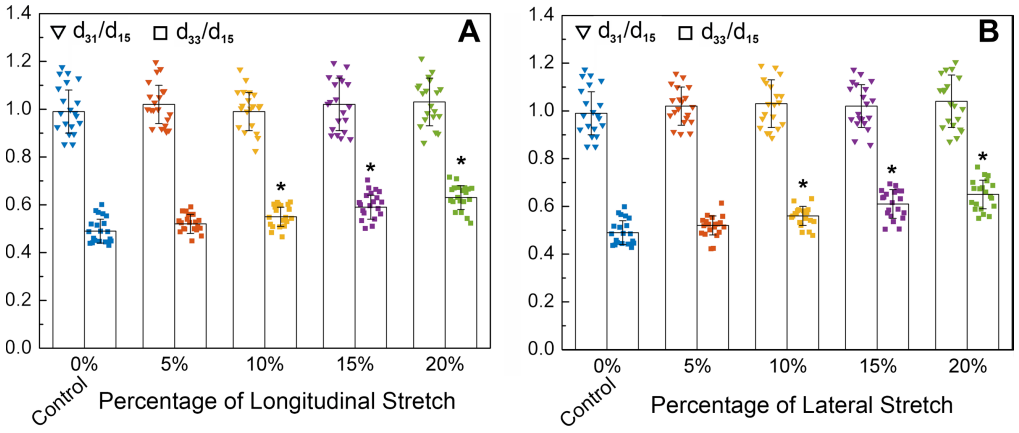

Fig. 5. Bar plot of the extracted ratio values of tensor components (d_{31}/d_{15} and d_{33}/d_{15}) in myosin filaments from (A) longitudinally stretched cardiomyocytes (d_{31}/d_{15} = 0.99 ± 0.09, 1.02 ± 0.08, 0.99 ± 0.08, 1.02 ± 0.11 and 1.03 ± 0.10; d_{33}/d_{15} = 0.49 ± 0.05, 0.52 ± 0.04, 0.55 ± 0.04, 0.59 ± 0.05 and 0.63 ± 0.05). (B) Laterally stretched cardiomyocytes, (d_{31}/d_{15} = 0.99 ± 0.09, 1.02 ± 0.08, 1.03 ± 0.10, 1.02 ± 0.09 and 1.04 ± 0.11; d_{33}/d_{15} = 0.49 ± 0.05, 0.52 ± 0.04, 0.56 ± 0.04, 0.61 ± 0.06 and 0.65 ± 0.06.). (sample size n = 20 measurements /group: 6 plates of cells were prepared for each longitudinal and lateral stretch group. 2-4 measurements were made for each plate. There was no statistical difference between the 6 plates in each group. Bars represent mean ± SD. One-way ANOVA followed by Student's t-test was used to compare different groups, *P < 0.05 vs. Control.)

3.3 Dynamic response of cardiomyocytes to mechanical tension

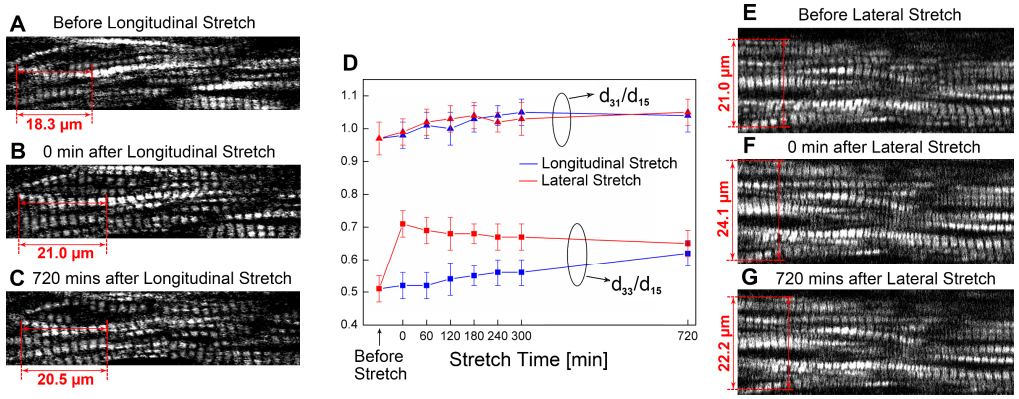

Fig. 6. Linearly polarized SHG images of cells before and after stretch: (A-C) longitudinal stretch and (E-G) lateral stretch. (D) The temporal response of the nonlinear susceptibility tensor components of myosin filaments after the cells were stretched by 15%. (Sample size n =

20 /group: 5 plates of cells were prepared for each longitudinal and lateral stretch group. 4 measurements were made for each plate. Bars represent mean ± SD).

The dynamic changes in the ratio of the nonlinear susceptibility tensor components over time in response to mechanical tension were studied. In view of the high mortality rate at 20% stretch, the cardiomyocytes were stretched to 15% either longitudinally or laterally. Figures 6(A) and 6(C), respectively, show the linearly polarized SHG images of cardiomyocytes after longitudinal and lateral stretch. After being stretched longitudinally and laterally, the cells had an instant increase in sarcomeric length and cross-sectional width, respectively, and the sarcomeric length and cross-sectional width gradually recovered under sustained stretch. The value of d_{31}/d_{15} remained virtually unchanged at approximately 1.00; however, the value of d_{33}/d_{15} obviously increased over time in both longitudinal and lateral stretch. When cardiomyocytes were stretched longitudinally, the value of d_{33}/d_{15} gradually increased from 0.50 ± 0.04 to 0.62 ± 0.05 in contrast to the immediate increase followed by a gradual recovery of sarcomeric length. When cardiomyocytes were stretched laterally, the value of d_{33}/d_{15} had an instant increment from 0.50 ± 0.04 to 0.70 ± 0.04, and the value decreased to 0.65 ± 0.04 during stretch sustained for 720 minutes. When cardiomyocytes were stretched laterally, the decrease in the value of d_{33}/d_{15} with time was consistent with the gradual recovery of the cross-sectional width of cells. By using the curve-fitting method, we also estimated the length of myosin filaments from the SHG images obtained from our cell stretch experiment. The results show that the length gradually increased after longitudinal stretch: The length of myosin filaments was 1.69 ± 0.11 μm, 1.74 ± 0.14 μm, and 1.83 ± 0.14 μm before stretching, 0 minutes after stretching, and 720 minutes after stretching, respectively.

4. Discussion

Heart weight to body weight ratios (Fig. 3(E)) increased significantly in our volume and pressure overload models. According to current thinking on hypertrophy, the increase in mass and volume during hypertrophy is due to the addition of new sarcomeres, without any change in sarcomeric length [20,21]. Our data agree with this thinking, showing no significant changes in sarcomeric length in hypertrophic hearts. Our data mainly revealed the structural differences in the polarization spectra by permitting a comparison between the ratios of the tensor components. The values of d_{31}/d_{15} (Fig. 4(B)) remained approximately 1.00 in normal and volume and pressure overload animal models, demonstrating that the Kleinman condition was valid in both the normal and the overload models. Our retrieved values (d_{31}/d_{15} and d_{33}/d_{15}) in normal myocardial tissues were close to the data reported by Odin and Tiaho [4,7]. However, the values of d_{33}/d_{15} were significantly increased in both volume- and pressure-overloaded myocardial tissues. The latest findings in the literature show that there is not necessarily a connection between sarcomeric length and the ratio of the nonlinear susceptibility tensor components [9]. Our findings demonstrate that in volume and pressure overloaded myocardia, the ratio of the nonlinear susceptibility tensor components may change in myosin filaments without changes in sarcomeric lengths.

The relationship between the ratio and the crystallographic structure of the myosin filaments has been reported in the literature: According to the theory of hyperpolarizability, bulk susceptibility is derived from the coherent summation of molecular hyperpolarizability [22]. Myosin filaments can be considered as cylindrically symmetrical molecules. The bulk susceptibility tensor components are related to the characteristic orientation angle θ (Fig. 7(B)).

$$\begin{aligned} d_{33} &= N_S \beta < \cos^3 \theta > \\ d_{15} &= d_{31} = \frac{1}{2} N_S \beta < \cos\theta \sin^2 \theta > \end{aligned} \tag{2}$$

Ns is the number density of active harmonophores, β is the molecule's hyperpolarizability, and the brackets <> indicate an orientation average. If the distribution of the effective molecular orientation is very narrow, the <> can be removed to obtain [23,24]:

$$D = \frac{<\cos^3\theta>}{<\cos\theta>} = \frac{d_{33}/d_{15}}{2 + d_{33}/d_{15}} = \cos^2\theta_e \quad (3)$$

where θ_e is an experimentally retrievable molecular orientation modeled as the helical pitch angle of the SHG source molecule (Fig. 7(B)). Equation (3) enables us, at the crystallographic level, to evaluate the helical pitch angle through d_{33}/d_{15} extracted from the polarization spectra. The value of the fitting parameter d_{33}/d_{15} in the normal myocardial tissues was measured to be 0.68 in this research, and the corresponding helical pitch angle was 61°, which is a close approximation of the angle of each helix relative to the main axis as obtained by X-ray diffraction [7,23,24]. Based on the single myosin spiral parameters (helix pitch P = 0.55 nm and diameter R = 0.44 nm) and using $\tan\theta = \pi * R / P$, the pitch angle obtained by X-ray diffraction is calculated to be about 68°. Therefore, our animal experiment results demonstrate that the volume or pressure overload-related structural changes in myosin filaments at the crystallographic level can be studied dynamically by calculating the ratio of the nonlinear susceptibility tensor components (d_{33}/d_{15}) obtained from PR-SHG microscopy.

Using a cell stretch-based hypertrophic model, our coauthor Dr. Thomas Borg observed an increase in the expression of protein turnover in stretched cardiomyocytes [25]. Recently, using a similar model, we captured sarcomeric addition under stretch. The means of sarcomeric addition in our model are similar to the behavior assumed from observation of in vivo hypertrophic models [16]. Therefore, our cell culture and stretch model can simulate the mechanics in the process of real cardiac hypertrophy.

The cell stretch data (Fig. 5 and Fig. 6) demonstrate the changes in d_{33}/d_{15} under mechanical tension. Our data show that the volume and pressure overload mimicked by mechanical stretch can lead to a significant increase in the value of d_{33}/d_{15}. It is worth noting that when no stretch was applied, the value of d_{33}/d_{15} was significantly smaller in stretch-free cardiomyocytes (0.49 ± 0.05) than the value in normal myocardia (0.69 ± 0.06) (Fig. 5). This may have been because the cardiomyocytes cultured on grooved PDMS substrate lacked the mechanical tension found in real myocardium. There is evidence that neonatal rat ventricular cardiomyocytes cultured on a soft substrate will show reduced contraction amplitude and frequency compared with the cells in vivo [26,27].

Mechanical tension mediates the structural remodeling of myosin filaments through intracellular cytoskeleton complexes associated with the sarcomeres (e.g., α-actinin, paxillin, titin and myosin binding protein C) [28,29]. The extensibility of the myosin filaments we observed in our overload-mimicking stretching model has been confirmed [10,30]: Changes in myosin filament length in volume- and pressure-overloaded myocardium were reported [31]. Although this length cannot be measured accurately, our previous discussion suggests that changes in the mean harmonophore orientation angle (Fig. 7(B)), which is related to the length changes, can be quantified by PR-SHG microscopy.

As 15% stretch was applied (Fig. 6), the value of d_{33}/d_{15} increased over time in both longitudinal and lateral stretch, but the responses of cardiomyocytes to longitudinal and lateral stretch differed. When cardiomyocytes were stretched longitudinally, the sarcomeric length immediately increased, but the value of d_{33}/d_{15} increased slowly over time. This suggests that the structural changes at the crystallographic level in the myosin filaments caused by longitudinal mechanical tension do not occur instantaneously, and the value of d_{33}/d_{15} is not related to sarcomeric length (This result is consistent with the reports by Sebastian and associates [9]). When cardiomyocytes were stretched laterally, an instantaneous increase of d_{33}/d_{15} was detected, and the trend of change in d_{33}/d_{15} was synchronized with the

change of cell cross-sectional width. This indicates that the crystallographic structure of myosin filament was more sensitive to lateral stretch than longitudinal stretch.

In our cell culture experiments when the cardiomyocytes were longitudinally stretched, titin, as a part of the stress responsive machinery, was the first sarcomeric component to respond to the tension. Titin elongated due to its spring-like property; the immediate increase in the sarcomeric length was attributable to titin [32]. The viscoelastic myosin filaments are typically modeled as a mechanical component aligned in series with titin. The delayed response of the myosin filaments was reflected in the delayed increase in the value of d_{33}/d_{15}, as shown in Fig. 6(D). As titin and the cytoskeleton gradually transferred the tension to myosin [33,34], the myosin coil was gradually stretched (the pitch angle was reduced correspondingly) and thus caused a gradual increase in the value of d_{33}/d_{15} from 0.49 to 0.64. The model is consistent with the experimental data in Fig. 6: The value of d_{33}/d_{15} did not increase immediately after cells were stretched, but gradually increased as the tension shifted.

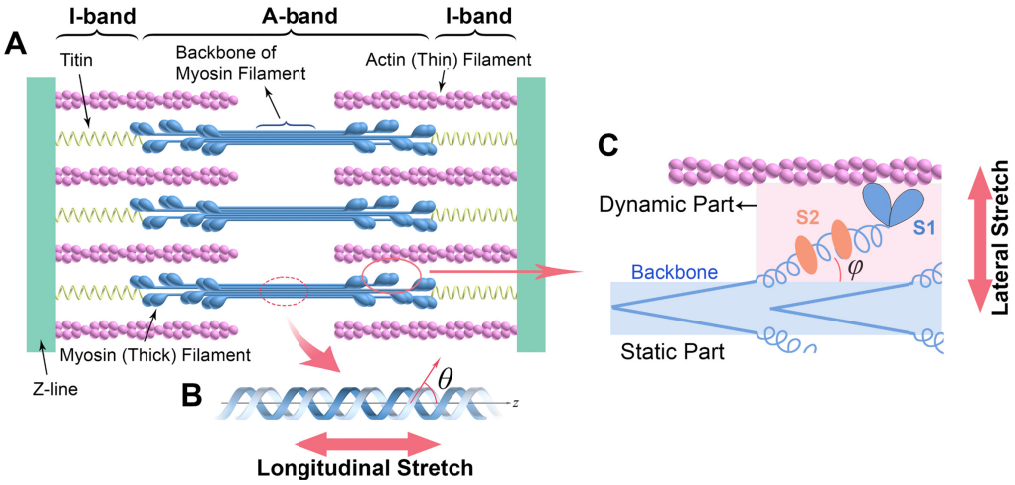

Fig. 7. (A) Schematic of a single sarcomere structure. (B) The myosin coil is made up of two alpha-intertwined helices. The θ is the mean harmonophore orientation angle. (C) The structure of a full-length myosin molecule was composed of the myosin coil (static parts), and a hinge region (S2) connects the two myosin heads (S1) with the myosin coil; S1 and S2 form the dynamic part. The model of double-headed rigor S1 extends from the myosin filament backbone to attach to actin to form the crossbridge.

Yoshikaway and associates reported that the passive stiffness of cardiomyocytes in the transverse direction increased significantly in hypertrophied rat hearts, and that the (residual) crossbridge is the main factor leading to increased passive stiffness [35]. This report suggests that the cross-bridge contributes to support the transverse mechanical load. When the cardiomyocytes were laterally stretched, the tension was directly exerted on the cross-bridge formed between myosin filaments and the actin filaments. The myosin molecule can be modeled with a static part (the myosin coil, which lies on the backbone of the myosin filament) and a dynamic part (S1 and S2, which extend from the main myosin filament body to attach to the actin filament) (Fig. 7). An angle φ is formed between the static part and the dynamic part, and the angle varies with different physiological states [36]. The sliding of myosin heads on actin changes the angle between the static and the dynamic parts. It has been demonstrated that the PR-SHG microscope is sensitive to the physiological states of a myosin molecule that are characterized by different angles of φ [8,9]. According to numerical simulation results, a 20-degree increment of the angle φ can trigger a significant increase in d_{33}/d_{15} [8]. Consequently, we hypothesize that during hypertrophy, the changes in the myosin head orientation in response to the mechanical tension is one of the causes of changes in the

value of d_{33}/d_{15}. An instantaneous change in the value of d_{33}/d_{15} demonstrates that there is no sarcomeric component like titin that can buffer the initial lateral tension.

Our data cannot be used to distinguish the effects of the changes in angle θ and φ during hypertrophy; however, our data demonstrate that hypertrophy may cause permanent changes at the crystallographic level in the myosin filaments. These changes cannot be revealed using conventional microscopic techniques and thus have not been reported in the literature. But these changes may be used to explore the transition from physiological to pathological hypertrophy; the latter has the potential to lead heart failure.

5. Conclusion

According to our experimental data, both pregnancy-induced volume overload and transverse-aortic constriction-induced pressure overload led to a significant increase in the ratio value of the d_{33}/d_{15} in myosin filament. And we have proved by cell stretch experiment that mechanical tension is the cause that leads to the increase of d_{33}/d_{15}. In addition, we explored the relationship between the structural changes in myosin filament and the changes in the ratio of the nonlinear susceptibility tensor components under mechanical tension. Considering that the volume overload and pressure overload are important causes of cardiac hypertrophy, the findings in this paper can be used for early diagnosis of cardiac hypertrophy induced by volume or pressure overload.

Funding

National Institutes of Health through SC COBRE (P20RR021949 and P20GM130451); R01 funding (R01HL124782 and R01HL144927); National Science Foundation EPSCoR Program (OIA-1655740); National Natural Science Foundation of China (61775148).

Disclosures

The authors declare that there are no conflicts of interest related to this article.

References

1. P. J. Campagnola and L. M. Loew, "Second-harmonic imaging microscopy for visualizing biomolecular arrays in cells, tissues and organisms," Nat. Biotechnol. **21**(11), 1356–1360 (2003).
2. W. Mohler, A. C. Millard, and P. J. Campagnola, "Second harmonic generation imaging of endogenous structural proteins," Methods **29**(1), 97–109 (2003).
3. X. Y. Dow, E. L. DeWalt, S. Z. Sullivan, P. D. Schmitt, J. R. W. Ulcickas, and G. J. Simpson, "Imaging the nonlinear susceptibility tensor of collagen by nonlinear optical stokes ellipsometry," Biophys. J. **111**(7), 1361–1374 (2016).
4. C. Odin, T. Guilbert, A. Alkilani, O. P. Boryskina, V. Fleury, and Y. Le Grand, "Collagen and myosin characterization by orientation field second harmonic microscopy," Opt. Express **16**(20), 16151–16165 (2008).
5. C. H. Yu, N. Langowitz, H. Y. Wu, R. Farhadifar, J. Brugues, T. Y. Yoo, and D. Needleman, "Measuring microtubule polarity in spindles with second-harmonic generation," Biophys. J. **106**(8), 1578–1587 (2014).
6. A. Tuer, S. Krouglov, R. Cisek, D. Tokarz, and V. Barzda, "Three-dimensional visualization of the first hyperpolarizability tensor," J. Comput. Chem. **32**(6), 1128–1134 (2011).
7. F. Tiaho, G. Recher, and D. Rouède, "Estimation of helical angles of myosin and collagen by second harmonic generation imaging microscopy," Opt. Express **15**(19), 12286–12295 (2007).
8. V. Nucciotti, C. Stringari, L. Sacconi, F. Vanzi, L. Fusi, M. Linari, G. Piazzesi, V. Lombardi, and F. S. Pavone, "Probing myosin structural conformation in vivo by second-harmonic generation microscopy," Proc. Natl. Acad. Sci. U.S.A. **107**(17), 7763–7768 (2010).
9. S. Schürmann, F. von Wegner, R. H. Fink, O. Friedrich, and M. Vogel, "Second harmonic generation microscopy probes different states of motor protein interaction in myofibrils," Biophys. J. **99**(6), 1842–1851 (2010).
10. I. Schwaiger, C. Sattler, D. R. Hostetter, and M. Rief, "The myosin coiled-coil is a truly elastic protein structure," Nat. Mater. **1**(4), 232–235 (2002).
11. S. Psilodimitrakopoulos, P. Loza-Alvarez, and D. Artigas, "Fast monitoring of in-vivo conformational changes in myosin using single scan polarization-SHG microscopy," Biomed. Opt. Express **5**(12), 4362–4373 (2014).
12. S. Roth and I. Freund, "Second harmonic generation in collagen," J. Chem. Phys **70**(4), 1637–1643 (1979).
13. Y. H. Shao, H. H. Liu, T. Ye, T. Borg, J. Qu, X. Peng, and Z. B. Gao, "3D myofibril imaging in live cardiomyocytes via hybrid SHG-TPEF microscopy," Proc. SPIE **7903**, 79030F (2011).

14. H. A. Rockman, R. S. Ross, A. N. Harris, K. U. Knowlton, M. E. Steinhelper, L. J. Field, J. Ross, Jr., K. R. Chien, and K. R. Chien, "Segregation of atrial-specific and inducible expression of an atrial natriuretic factor transgene in an in vivo murine model of cardiac hypertrophy," Proc. Natl. Acad. Sci. U.S.A. **88**(18), 8277–8281 (1991).
15. Z. Ma, R. K. Pirlo, Q. Wan, J. X. Yun, X. Yuan, P. Xiang, T. K. Borg, and B. Z. Gao, "Laser-guidance-based cell deposition microscope for heterotypic single-cell micropatterning," Biofabrication **3**(3), 034107–034116 (2011).
16. H. Yang, L. P. Schmidt, Z. Wang, X. Yang, Y. Shao, T. K. Borg, R. Markwald, R. Runyan, and B. Z. Gao, "Dynamic myofbrillar remodeling in live cardiomyocytes under static stretch," Sci. Rep. **6**(1), 20674–20686 (2016).
17. J. Sadoshima, L. Jahn, T. Takahashi, T. J. Kulik, and S. Izumo, "Molecular characterization of the stretch-induced adaptation of cultured cardiac cells," J. Biol. Chem. **267**(15), 10551–10560 (1992).
18. A. Leychenko, E. Konorev, M. Jijiwa, and M. L. Matter, "Stretch-induced hypertrophy activates NFkB-mediated VEGF secretion in adult cardiomyocytes," PLoS One **6**(12), e29055 (2011).
19. T. Boulesteix, E. Beaurepaire, M. P. Sauviat, and M. C. Schanne-Klein, "Second-harmonic microscopy of unstained living cardiac myocytes: measurements of sarcomere length with 20-nm accuracy," Opt. Lett. **29**(17), 2031–2033 (2004).
20. F. Morady, M. M. Laks, and W. W. Parmley, "Comparison of sarcomere lengths from normal and hypertrophied inner and middle canine right ventricle," Am. J. Physiol. **225**(6), 1257–1259 (1973).
21. P. Anversa, R. Ricci, G. Olivetti, and G. Olivetti, "Quantitative structural analysis of the myocardium during physiologic growth and induced cardiac hypertrophy: A review," J. Am. Coll. Cardiol. **7**(5), 1140–1149 (1986).
22. A. Leray, L. Leroy, Y. Le Grand, C. Odin, A. Renault, V. Vié, D. Rouède, T. Mallegol, O. Mongin, M. H. Werts, and M. Blanchard-Desce, "Organization and orientation of amphiphilic push-pull chromophores deposited in Langmuir-Blodgett monolayers studied by second harmonic generation and atomic force microscopy," Langmuir **20**(19), 8165–8171 (2004).
23. S. Psilodimitrakopoulos, I. Amat-Roldan, P. Loza-Alvarez, and D. Artigas, "Estimating the helical pitch angle of amylopectin in starch using polarization second harmonic generation microscopy," J. Opt. **12**(8), 084007–084013 (2010).
24. S. Psilodimitrakopoulos, D. Artigas, G. Soria, I. Amat-Roldan, A. M. Planas, and P. Loza-Alvarez, "Quantitative discrimination between endogenous SHG sources in mammalian tissue, based on their polarization response," Opt. Express **17**(12), 10168–10176 (2009).
25. D. G. Simpson, W. W. Sharp, T. K. Borg, R. L. Price, L. Terracio, and A. M. Samarel, "Mechanical regulation of cardiac myocyte protein turnover and myofibrillar structure," Am. J. Physiol. **270**(4), C1075–C1087 (1996).
26. N. Hersch, B. Wolters, G. Dreissen, R. Springer, N. Kirchgeßner, R. Merkel, and B. Hoffmann, "The constant beat: cardiomyocytes adapt their forces by equal contraction upon environmental stiffening," Biol. Open **2**(3), 351–361 (2013).
27. G. B. Belostotskaya and T. A. Golovanova, "Characterization of contracting cardiomyocyte colonies in the primary culture of neonatal rat myocardial cells," Cell Cycle **13**(6), 910–918 (2014).
28. M. K. Miller, H. Granzier, E. Ehler, and C. C. Gregorio, "The sensitive giant: the role of titin-based stretch sensing complexes in the heart," Trends Cell Biol. **14**(3), 119–126 (2004).
29. P. Tonino, B. Kiss, J. Strom, M. Methawasin, J. E. Smith 3rd, J. Kolb, S. Labeit, and H. Granzier, "The giant protein titin regulates the length of the striated muscle thick filament," Nat. Commun. **8**(1), 1041–1052 (2017).
30. K. Wakabayashi, Y. Sugimoto, H. Tanaka, Y. Ueno, Y. Takezawa, and Y. Amemiya, "X-ray Diffraction evidence for the extensibility of actin and myosin filaments during muscle contraction," Biophys. J. **67**(6), 2422–2435 (1994).
31. I. Torre, A. González-Tendero, P. García-Cañadilla, F. Crispi, F. García-García, B. Bijnens, I. Iruretagoyena, J. Dopazo, I. Amat-Roldán, and E. Gratacós, "Permanent cardiac sarcomere changes in a rabbit model of intrauterine growth restriction," PLoS One **9**(11), e113067–e113075 (2014).
32. R. Horowits and R. J. Podolsky, "The positional stability of thick filaments in activated skeletal muscle depends on sarcomere length: evidence for the role of titin filaments," J. Cell Biol. **105**(5), 2217–2223 (1987).
33. R. Knöll, M. Hoshijima, and K. Chien, "Cardiac mechanotransduction and implications for heart disease," J. Mol. Med. (Berl.) **81**(12), 750–756 (2003).
34. M. Helmes, K. Trombitás, T. Centner, M. Kellermayer, S. Labeit, W. A. Linke, and H. Granzier, "Mechanically driven contour-length adjustment in rat cardiac titin's unique N2B sequence: titin is an adjustable spring," Circ. Res. **84**(11), 1339–1352 (1999).
35. W. Sumita Yoshikawa, K. Nakamura, D. Miura, J. Shimizu, K. Hashimoto, N. Kataoka, H. Toyota, H. Okuyama, T. Miyoshi, H. Morita, K. Fukushima Kusano, T. Matsuo, M. Takaki, F. Kajiya, N. Yagi, T. Ohe, and H. Ito, "Increased passive stiffness of cardiomyocytes in the transverse direction and residual actin and myosin cross-bridge formation in hypertrophied rat hearts induced by chronic β-adrenergic stimulation," Circ. J. **77**(3), 741–748 (2013).
36. R. S. Goody, "The missing link in the muscle cross-bridge cycle," Nat. Struct. Biol. **10**(10), 773–775 (2003).